Contrib Mineral Petrol (2014) 167:990
DOI 10.1007/s00410-014-0990-x

ORIGINAL PAPER

Titanium- and water-rich metamorphic olivine in high-pressure serpentinites from the Voltri Massif (Ligurian Alps, Italy): evidence for deep subduction of high-field strength and fluid-mobile elements

Jan C. M. De Hoog · Keiko Hattori · Haemyeong Jung

Received: 18 April 2013 / Accepted: 25 October 2013 / Published online: 11 March 2014

Abstract Titanium- and water-rich metamorphic olivine (Fo 86–88) is reported from partially dehydrated serpentinites from the Voltri complex, Ligurian Alps. The rocks are composed of mostly antigorite and olivine in addition to magnetite, chlorite, clinopyroxene and Ti-clinohumite. In situ secondary ion mass spectrometry (SIMS) data show that metamorphic olivine has very high and strongly correlated H_2O (up to 0.7 wt%) and TiO_2 contents (up to 0.85 wt%). Ti-rich olivine shows colourless to yellow pleochroism. Olivine associated with Ti-clinohumite contains low Ti, suggesting that Ti-rich olivine is not the breakdown product of Ti-clinohumite. Fourier transform infrared spectroscopy (FTIR) absorption spectra show peaks of serpentine, Ti-clinohumite and OH-related Si vacancies. Combining FTIR and SIMS data, we suggest the presence of clustered planar defects or nanoscale exsolutions of Ti-clinohumite in olivine. These defects or exsolutions contain more H_2O ($x \sim 0.1$ in the formula $4Mg_2SiO_4{\cdot}(1-x)Mg(OH,F)_2{\cdot}xTiO_2$) than Ti-clinohumite in the sample matrix ($x = 0.34$–0.46). In addition to TiO_2 and H_2O, secondary olivine contains significant Li (2–60 ppm), B (10–20 ppm), F (10–130 ppm) and Zr (0.9–2.1 ppm). It is enriched in ^{11}B ($\delta^{11}B = +17$ to $+23$ ‰). Our data indicate that secondary olivine may play a significant role in transporting water, high-field strength and fluid-mobile elements into the deeper mantle as well as introduce significant B isotope anomalies. Release of hydrogen from H_2O-rich olivine subducted into the deep mantle may result in strongly reduced mantle domains.

Keywords Metamorphic olivine · Clinohumite · Serpentinite · High-pressure metamorphism · Subduction recycling of elements · Voltri Massif

Communicated by J. L. R. Touret.

J. C. M. De Hoog (✉)
Grant Institute, School of GeoSciences, University of Edinburgh, West Mains Road, Edinburgh EH9 3JW, UK
e-mail: ceesjan.dehoog@ed.ac.uk

K. Hattori
Department of Earth Sciences, University of Ottawa, Ottawa, Canada

H. Jung
School of Earth and Environmental Sciences, Seoul National University, Seoul, South Korea

Introduction

Serpentinites play an important role in the cycling of water and fluid-mobile elements in subduction zones (Scambelluri et al. 2004a; John et al. 2011; e.g., Kodolanyi et al. 2012). Hydrated oceanic crust will dehydrate upon subduction and release fluids and fluid-mobile elements to the overlying mantle wedge (Ulmer and Trommsdorff 1995). This fluid causes hydration of the overlying forearc-mantle peridotites, producing more serpentinites at the base of the mantle wedge (Hattori and Guillot 2003). These forearc-mantle serpentinites have high H_2O contents (up to 13 wt%) and are enriched in fluid-mobile metals, such as As, Sb and Pb (e.g., Hattori and Guillot 2007; Savov et al. 2007). Their downward movement by mantle flow eventually causes the serpentinites to dehydrate at a depth of $\sim$100 km, releasing water and fluid-mobile elements into the interior of the mantle wedge, where they induce partial melting related to arc magmatism (Ulmer and Trommsdorff 1995). Mantle-wedge serpentinites thus act as a sponge transferring fluid-mobile elements from the forearc to subarc mantle (Hattori and Guillot 2003).

Dehydration is accompanied by the generation of secondary, metamorphic olivine. It is generally thought that most fluid-mobile elements will be lost from the dehydrating serpentinite to the mantle wedge during their dehydration. However, nominally anhydrous minerals (NAMs) such as olivine may contain considerable amounts of water in crystal defects in their structure (e.g., Kitamura et al. 1987; Khisina and Wirth 2002; Peslier 2010) and deep subduction of B and Li by olivine and clinohumite was suggested Scambelluri et al. (2004b). Hence, secondary olivine may potentially introduce large amounts of water and fluid-mobile elements to deeper depths, which has important implications for rheology of mantle peridotites, compositions of mantle fluids and partial melts, and deep recycling of elements into the mantle. To evaluate the retention of elements during serpentinite dehydration in the mantle, we examined the compositions of secondary olivine grains in the Erro-Tobbio peridotite from the Voltri Massif, which formed during serpentinite dehydration at depths of about 75 km (Scambelluri et al. 1995).

Sample description and petrography

Samples were collected from the Erro-Tobbio metaperidotite in the Voltri Massif (Ligurian Alps, Italy) where the rocks are well exposed along the Gorzente River (Piccardo et al. 1988; Scambelluri et al. 1991, 1995). The metaperidotite is a slice of abyssal peridotite that was serpentinised on the pre-Jurassic ocean floor and underwent partial dehydration during its subduction up to pressures of 25 kbar in Cretaceous time (Cimmino et al. 1979; Scambelluri et al. 1991, 1995). This dehydration resulted in the formation of secondary olivine and minor humite minerals, which form discontinuous veins of several centimetres width in serpentinites (Scambelluri et al. 1995).

The sample which is the focus of this paper (*VT8-3,* 44°33.677′N, 8°48.907′E), is a chlorite-bearing serpentinite that shows a prominent foliation defined by the alignment of antigorite and chlorite and bands of secondary olivine and clinohumite (Fig. 1a–f). It contains magnetite and acicular diopside as well as rare porphyroclastic augitic clinopyroxene. Olivine (Ol) occurs as large but heavily fractured grains as well as fine-grained domains. They contain abundant inclusions of low-Ti magnetite (Mag), confirming their secondary origin. Fine-grained needle-like diopside is associated with olivine and clinohumite. Magnetite is often finely disseminated and associated with clinohumite-rich domains.

Several generations of secondary olivine are recognised based on microtexture and mineral chemistry. The early metamorphic olivine is Ti-poor and forms porphyroclastic discrete grains in an antigorite matrix and less commonly in Ol–Chu–Mag veins. The second generation also forms porphyroclastic discrete grains in the antigorite matrix, but it is Ti-rich (up to 0.8 wt%). Locally, it forms overgrowths around earlier Ti-poor olivine. The third-generation olivine is fine-grained Ti-poor olivine forming the bulk of the Ol–Chu–Mag veins, probably the result of dynamic recrystallisation during late-stage deformation. This also resulted in recrystallisation of fine-grained humite-group minerals (Fig. 1c). In addition, large cm-sized masses of heavily fractured olivine occur, which appear to predate all other generations.

Three different sections were prepared from a single-hand specimen: a thick (~100 μm) section suitable for LA–ICP–MS analysis (VT8-3A), a regular polished thin section (VT8-3B) and a double-polished thick (~150 μm) section suitable for Fourier transform infrared spectroscopy (FTIR) analysis (VT8-3C).

Analytical methods

Electron probe microanalysis (EPMA)

Major and minor elements were measured by electron probe Cameca SX-100 at EMMAC, University of Edinburgh, using a dedicated high-precision set-up developed for low concentrations of minor elements in olivine. Accelerating voltage was 20 kV with a defocused 5-μm beam. Mg, Si and Fe were measured at 10 nA for 60 s, whereas minor elements were measured at 80 nA for 240 s (Na, Al, Ca, Cr) or 120 s (Mn, Ni). Pure forsterite and fayalite were used to calibrate Si, Mg and Fe, respectively, in addition to wollastonite, Mg spinel, jadeite and pure metals for remaining elements. Accuracy and precision were monitored by repeated analysis of San Carlos olivine from USGS (USNM# 111312/44; Jarosewich et al. 1980), in-house olivine standard DC0212 (see De Hoog et al. 2010, for preparation and details) and an in-house Cr-diopside standard, the latter to monitor elements, which are low in olivine (Na, Al, Ca, Cr). Additional analyses were performed with the same set-up but with shorter counting times on other minerals (humite group, serpentine, oxides, some olivines).

Additional mineral analyses were done at Carleton University, Ottawa, using a CAMEBAX MBX electron probe in the wavelength dispersive mode. Counting times were 15–20 s per element, except for Ni (40 s). A 15-kV accelerating voltage and a 20-nA beam current were applied. The calibration used orthoclase (Si), wollastonite (Ca), synthetic spinel (Al), synthetic Cr_2O_3 (Cr), forsterite (Mg), synthetic $MnTiO_3$ (Mn and Ti), albite (Na), fayalite (Fe in silicates), metallic Ni (Ni) and synthetic Fe_2O_3 (Fe in oxides). Results of both EPMA laboratories were in excellent agreement.

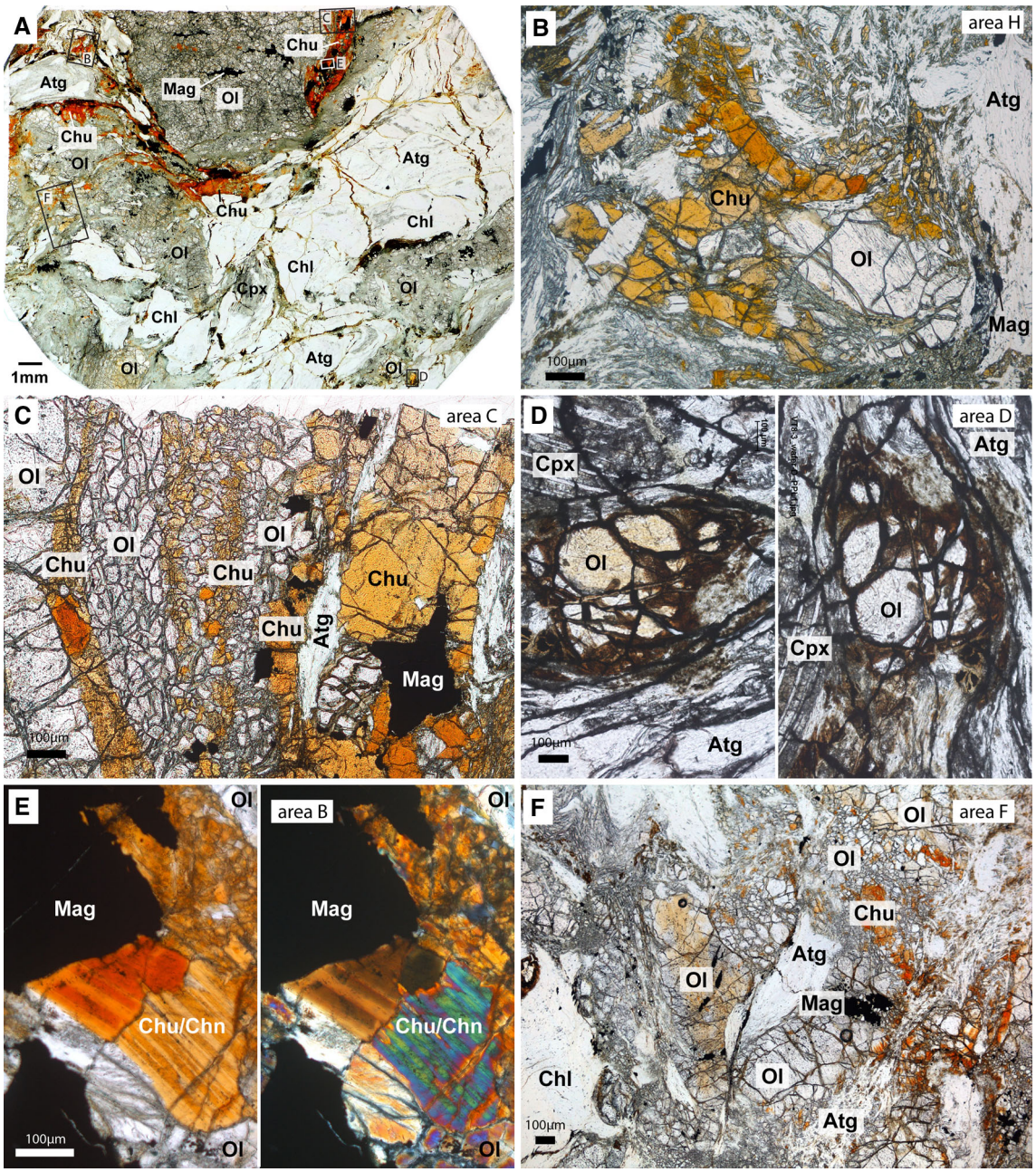

Fig. 1 Petrography of Voltri serpentinite (section VT8-3B). *Scale bars* in *bottom-left corners* of each photograph are 100 µm wide except for A (1 mm). Rectangles indicate locations of detailed photographs. Note that B, E and F are 90° rotated. The area numbers indicated in the detailed photographs match those of the grain numbers in the compositional tables (Tables 1, 2, 3, 4 and 5). Mineral abbreviations from Whitney and Evans (2010). **a** Transmitted light scanned image of thin section. **b** Clinohumite in contact with Ti-poor olivine porphyroclast in antigorite matrix. Some of the orange grains are chondrodite and humite (plane-polarised light). **c** Coarse-grained Ti-poor olivine and clinohumite recrystallised to fine-grained crystal aggregates. The *small orange grains* are dominantly clinohumite with about one-third chondrodite. Recrystallised olivine has low TiO_2 contents (plane-polarised light). **d** Titanium-rich olivine in antigorite matrix exhibiting *yellow* (*left*) to *colourless* (*right*) pleochroism (plane-polarised light). Also note the presence of exsolved and deformed clinopyroxene interpreted to be relic mantle pyroxene. **e** Chondrodite lamellae (*dark brown*) in clinohumite (*light brown*) in plane-polarised light (*left*) and under crossed polarisers exhibiting anomalous interference colours (*right*). **f** Porphyroclastic Ti-rich olivine (*yellowish*) associated with colourless Ti-poor porphyroclastic olivine (plane-polarised light)

Secondary ion mass spectrometry (SIMS)

Water contents and selected trace elements were measured by SIMS Cameca 4f at the Edinburgh Ion Microprobe Facility (EIMF), University of Edinburgh. Polished samples were gold coated and kept under high vacuum ($<5\times10^{-8}$ mbar) for at least 48 h prior to analyses. We used a 5-nA primary beam of negative ^{16}O ions accelerated

to 14.5 kV. Every spot was pre-sputtered for 3 min with 30-μm rastered beam, then spots were analysed with a 20-μm beam using a small field aperture to avoid stray H ions from the beam periphery entering the mass spectrometer. Depth of the analysis pits was <2 μm. This set-up allowed us to reach a background of ~50 ppm H_2O in San Carlos olivine, which value was subtracted from all subsequent water analyses. Collected isotopes are ^{1}H, ^{7}Li, ^{11}B, ^{19}F, ^{23}Na, ^{26}Mg, ^{27}Al, ^{30}Si, ^{39}K, ^{40}Ca, ^{41}K, ^{43}Ca, ^{44}Ca, ^{45}Sc, ^{46}Ti, ^{47}Ti, ^{48}Ti, ^{49}Ti, ^{51}V, ^{52}Cr, ^{53}Cr, ^{55}Mn, ^{88}Sr, ^{89}Y, ^{90}Zr using an energy window of 50 ± 25 V. Raw count rates were corrected for molecular interferences such as MgO^+ (mass 40–42), $MgOH^+$ (mass 41–43), SiO^+ (mass 44–46), $SiOH^+$ (mass 45–47), $MgMg^+$ (mass 48–52) and $MgSi^+$ (52–56). Concentrations of trace elements were calculated against GSE1-G (Jochum and Nohl 2008) using Si as an internal standard. Water concentrations of olivine and humite-group minerals were calibrated using a set of in-house basaltic glass standards ranging in concentration from 0.32 to 4.63 wt% H_2O (Hall 1998; Shishkina et al. 2010). The use of basalt standards may introduce a bias in measured olivine and humite-group mineral water contents, but the measured values for the latter are very close to those calculated from stoichiometry. This suggests that matrix-induced fraction for olivine is likely small. The presence of water-bearing inclusions was monitored using the $^{1}H/^{30}Si$ signal, but no such inclusions were detected.

Boron isotope compositions were measured using a Cameca 1270 secondary ion mass spectrometry (SIMS) at EIMF, University of Edinburgh. A primary beam of $^{16}O_2^-$ with a current of 5 nA was used with a spot size of ca. 15 × 20 μm. Secondary ions were extracted at a constant 10-kV voltage and collected by a single electron multiplier measuring ^{10}B and ^{11}B alternately for 4 and 2 s, respectively, for a total of 900 s per analysis. The area for the analysis was pre-sputtered for about 3 min, which included ion beam centring time. No energy filtering of secondary ions was applied. A small image field (50 μm) and field aperture (20 μm) ensured maximum intensity whilst minimising the effect of secondary ion beam aberrations. Mass resolution ($\Delta m/m$) of ca. 1,200 was used to avoid interferences from $^{10}B^{1}H$ on ^{11}B and $^{9}Be^{1}H$ on ^{10}B signals.

Instrumental mass fractionation was corrected using GSD1-G basalt ($^{11}B/^{10}B$ ratio of 4.0849 based on a $\delta^{11}B$ value of +10.2 ± 0.5 ‰ reported by Jochum and Nohl 2008), GOR128-G komatiite (+13.6 ± 0.2 ‰; Rosner and Meixner 2004) and StHs6/80-G dacite (−4.4 ± 0.3 ‰; Rosner et al. 2008). As small matrix-dependent fractionations were observed between these glasses (−2.6 ‰ for GOR128-G komatiite and −1.6 ‰ for StHs6/80-G relative to GSD1-G), we used komatiite GOR128-G as the primary standard, as it is closest in composition to olivine. Boron isotope compositions are presented as permil notation relative to SRM951 using the following equation: $\delta^{11}B_{sample} = 1{,}000 \times (R_{sample}/R_{STD} \times R^*_{STD}/R^*_{LSVEC} - 1)$ where R is the measured $^{11}B/^{10}B$ ratio and R* is the true $^{11}B/^{10}B$ ratio. The SRM951 $^{11}B/^{10}B$ ratio of 4.0437 was taken from Catanzaro et al. (1970).

Fourier transform infrared spectroscopy (FTIR)

FTIR was used to determine the structural position of hydroxyl in olivine on a doubly polished section of 150 μm thickness (VT8-3C). The section was kept in an oven at 120 °C for more than 1 day before the measurement. A Nicolet 6,700 instrument with a Continuum IR Microscope was used at the Tectonophysics Laboratory at SEES in Seoul National University. The water content within a single crystal was measured using an IR beam size of 30 × 30 μm. Nitrogen gas was flushed during the FTIR measurement to avoid measuring the moisture in the atmosphere. The measurements were carried out using an unpolarised light source, a KBr beam-splitter and an MCT detector. A series of 128 scans was averaged for each spectrum with a resolution of 4 cm^{-1}.

Laser ablation ICP–MS

Selected minerals were measured in thick section (VT8-3A) for their trace element contents by laser ablation ICP–MS in the Department of Earth Sciences at the University of Oxford using a custom-built New Wave 193 nm ArF Excimer laser system attached to a Thermo-Finnegan Element2 magnetic sector ICP–MS in low-resolution mode. Ablation took place in He atmosphere, and spot size was 90–180 μm. NIST SRM-612 was used for calibration (Pearce et al. 1997). Further details including identification and correction of molecular interferences for olivine can be found in De Hoog et al. (2010).

Electron backscatter diffraction (EBSD)

Electron backscatter diffraction (EBSD) analysis was performed using the HKL Channel five EBSD system on a Philips XL30CP SEM at EMMAC, University of Edinburgh, operating at 20-kV accelerating voltage with a beam current of ca. 1 nA and a 20-mm working distance with a tilt angle of 70°. For each point of the map, the diffraction pattern was collected and solved by the HKL software for the orientation. Prior to EBSD analysis, the sample (VT8-3A) was polished with colloidal silica in order to remove damage to the surface caused by prior mechanical polishing.

Table 1 Major element data of selected minerals by EPMA

Mineral	Ol1	Ol2	Chu	Hu	Chn	Atg	Mag	Cpx1	Cpx2
Section	VT8-3B	VT8-3B	VT8-3B	VT8-3B	VT8-3B	VT8-3B	VT8-3B	VT8-3B	VT8-3C
Grain	C-2	D-5	C-1	A-2	C-4	A-7	C-1	D-1	F-3
Laboratory codes	UoE	UoE	UoE	UoE	UoE	OU	UoE	OU	OU
SiO_2	40.03	39.26	36.53	34.92	32.69	41.54	0.17	51.26	54.46
TiO_2	<d.l.	0.861	4.72	5.39	7.76	0.01	0.41	0.40	0.01
Al_2O_3	<d.l.	<d.l.	<d.l.	<d.l.	0.01	2.56	0.05	5.46	0.05
Cr_2O_3	<d.l.	0.045	0.08	0.04	0.12	0.11	3.48	1.12	0.02
Fe_2O_3							63.93		
FeO	12.60	12.13	13.02	12.17	12.71	3.66	30.63	2.72	1.91
MnO	0.347	0.294	0.44	0.39	0.44	0.05	0.09	0.05	0.10
NiO	0.315	0.296	0.20	0.14	0.14	0.07	0.24	0.02	0.00
MgO	46.82	46.71	44.13	44.78	42.64	37.00	0.43	15.26	17.57
CaO	0.007	0.005	0.00	0.01	0.01	0.02	<d.l.	22.91	25.58
Na_2O	<d.l.	<d.l.	n.a.	n.a.	n.a.	<d.l.	n.a.	0.31	<d.l.
H_2O[b]	0.036	0.680	1.49	2.27	2.97	12.52	n.a.	n.a.	n.a.
Total	100.19	100.47	100.62	100.11	99.52	97.54	99.31	99.51	99.70
#(O,OH,F)	4	4	18	14	10	9	4	6	6
#Si	0.994	0.967	4.047	3.000	2.019	1.991	0.006	1.875	1.989
#Ti	0.001	0.016	0.393	0.349	0.361	0.000	0.012	0.011	0.000
#Al	0.000	0.000	0.000	0.000	0.001	0.144	0.002	0.235	0.002
#Fe^{3+}							1.855		
#Cr	0.000	0.001	0.007	0.003	0.006	0.004	0.106	0.032	0.001
#Fe^{2+}	0.262	0.250	1.206	0.874	0.657	0.147	0.988	0.083	0.058
#Mn	0.007	0.006	0.041	0.028	0.023	0.002	0.003	0.002	0.003
#Ni	0.006	0.006	0.018	0.010	0.007	0.003	0.008	0.001	0.000
#Mg	1.733	1.715	7.288	5.736	3.926	2.643	0.025	0.832	0.956
#Ca	0.000	0.000	0.000	0.001	0.001	0.001	0.000	0.898	1.000
#Na	0.000	0.000	0.000	0.000	0.000	0.000	0.000	0.022	0.000
#Cations	3.003	2.961	13.000	10.000	7.000	4.935	3.000	3.991	4.010
#OH	0.006	0.112	1.099	1.301	1.222	4.000			
Mg#	0.869	0.873	0.858	0.868	0.857	0.947	0.024	0.909	0.943
M/Si	2.02	2.06	2.21	2.33	2.47				
$x(TiO_2)$			0.46	0.35	0.38				

[a] Fe_2O_3 by stoichiometry; [b] H_2O by stoichiometry, except olivine by SIMS; Mg# = Mg/(Mg + Fe^{2+}); M/Si = (#cations –#Si)/#Si; $x(TiO_2)$ = value of x in general formula $nMg_2SiO_4.(1-x)Mg(OH)_2.xTiO_2$; <d.l. = less than detection limit; n.a. = not analysed. Atg = antigorite, Ol = olivine, Chu = clinohumite, Hu = humite, Chn = chondrodite, Mag = magnetite, Cpx = clinopyroxene, laboratory codes: UoE = University of Edinburgh, OU = Ottawa University

Mineral compositions

Olivine

Major and trace elements (EPMA)

Two types of secondary olivine are identified based on their chemistry (Table 1): low-Ti olivine (2–250 ppm Ti) and Ti-rich olivine (500–2,600 ppm Ti). The latter shows pleochroism from colourless to light yellow in plane-polarised transmitted light and usually occurs as small porphyroclasts within the antigorite matrix (Fig. 1d, f). Both types show identical EBSD patterns to olivine. Occasionally, high-Ti olivine forms rims around low-Ti grains (e.g., VT8-3C grain C, Table 2). Low-Ti olivine occurs as small porphyroclasts in the antigorite matrix, as large porphyroclastic olivine and as recrystallised fine-grained olivine that constitutes most of the Ol–Chu–Mag veins but also mantles Ti-poor and Ti-rich olivine porphyroclasts.

Apart from their variable TiO_2 contents, all olivines have very similar major element compositions spanning a narrow range of Fo contents (86.5–87.6 %), which is slightly lower than typical mantle olivine. NiO contents (0.23–0.39 wt%) are comparable to typical mantle olivine,

Table 2 Trace element and water contents of olivine by SIMS

Section	Grain	H_2O	Li	B	F	Al	Ca	Sc	Ti	V	Cr	MnO	Sr	Y	Zr
VT8-3A	A-1	1,785	17	14	29	317	75	n.a.	1,086	n.a.	n.a.	0.36	1.1	0.53	3.2
VT8-3A	A-2	2,090	22	16	34	463	98	n.a.	771	n.a.	n.a.	0.38	1.5	0.81	0.7
VT8-3A	B-2	338	47	10	9	55	27	n.a.	211	n.a.	n.a.	0.33	0.5	0.22	0.9
VT8-3A	C-1	684	5	17	16	2	39	n.a.	223	n.a.	n.a.	0.35	3.9	0.38	2.5
VT8-3A	E-1	817	5	11	16	1	26	n.a.	17	n.a.	n.a.	0.28	0.5	0.08	0.5
VT8-3A	F-1	590	34	11	18	32	24	n.a.	491	n.a.	n.a.	0.36	0.3	0.24	0.3
VT8-3B	A-1	655	12	15	12	1	23	34	124	1	33	0.31	2.4	0.55	0.7
VT8-3B	B-1	460	16	10	15	3	<1	40	114	3	43	0.34	0.9	0.24	0.3
VT8-3B	B-2	223	6	11	7	2	5	18	2	2	51	0.33	0.7	0.16	0.3
VT8-3B	C-2	363	17	9	5	2	7	40	80	3	34	0.35	0.7	0.17	0.2
VT8-3B	D-1	5,777	31	16	47	51	4	67	2,434	10	271	0.36	0.9	0.45	2.1
VT8-3B	D-2	4,784	39	16	31	31	8	82	2,036	11	265	0.36	0.9	0.36	1.8
VT8-3B	D-3	5,460	35	14	51	27	2	72	2,558	10	259	0.36	0.7	0.38	1.8
VT8-3B	D-4	1,689	44	14	15	22	3	117	535	9	301	0.35	0.8	0.37	0.9
VT8-3B	D-5	6,802	17	18	137	10	<1	42	4,545	11	199	0.30	0.5	0.43	2.4
VT8-3C	A-1	1,124	5	20	11	1	9	15	559	1	47	0.32	0.5	0.36	1.2
VT8-3C	A-2	1,017	6	20	24	5	11	15	611	2	51	0.34	0.4	0.28	1.4
VT8-3C	A-3	2,279	4	23	22	2	5	14	1,417	3	42	0.30	0.6	0.48	2.0
VT8-3C	B1-1c	537	33	12	27	1	9	28	211	4	125	0.30	0.5	0.19	0.3
VT8-3C	B1-2c	891	22	12	27	1	4	27	364	4	110	0.29	0.6	0.19	0.4
VT8-3C	B2-1c	140	13	15	10	1	3	94	14	8	184	0.29	0.5	0.21	0.4
VT8-3C	B5r	5,431	7	20	111	2	8	20	4,184	8	106	0.32	1.0	0.34	2.0
VT8-3C	B3r	4,535	12	14	64	2	3	36	2,263	8	123	0.29	0.5	0.22	0.7
VT8-3C	C-1	267	27	12	7	0	6	26	100	4	136	0.31	0.6	0.18	0.3
VT8-3C	I-1	151	27	12	6	1	7	34	9	3	67	0.28	0.6	0.19	0.3

All concentrations in ppm, except MnO in wt%

but NiO and Fo show no correlation. MnO contents are relatively high (0.26–0.43 wt%), which is in agreement with olivine being of secondary (metamorphic) origin. This is also supported by abundant inclusions of magnetite, which is a product of earlier serpentinisation. CaO contents are low but variable (0.001–0.029). Cr_2O_3 contents range from <.001 to 0.070 wt% but are on average higher in Ti-rich olivine than typical mantle olivine (0.017 and 0.005, respectively; De Hoog et al. 2010).

Ti-rich olivine shows a distinct Si deficiency in its calculated formula, as #Si is 0.995–1.005 in Ti-poor olivine but down to 0.970 in Ti-rich olivine (based on 4O, Table 1). This may be explained by the presence of defects or separate phases as exsolutions or inclusions, as indicated by FTIR spectra (Ti-clinohumite defects or exsolutions; In "Water content and structural position" section).

Trace elements (SIMS and LA–ICP–MS)

Selected olivines were analysed for trace elements by SIMS (Table 2). Many trace elements are enriched in Ti-rich olivines compared with Ti-poor olivines, e.g., F (15–51 vs. 5–35 ppm), Al (22–51 vs. 2–3 ppm), Sc (67–117 vs. 18–40 ppm), V (9–11 vs. 2–3 ppm), Cr (0.038–0.044 vs. 0.004–0.007 wt%), Y (0.7–0.9 vs. 0.2 ppm) and Zr (0.9–2.1 vs. 0.2–0.3 ppm). In contrast, Li and B contents show little difference (Li: 31–44 ppm in Ti-rich olivine and 6–17 ppm in regular olivine; B: 14–16 vs. 9–13 ppm).

Results from LA–ICP–MS (Table 3) are very similar to those measured by SIMS except Sc, V and Cr, which show lower values by 20–50 %. The discrepancies of these elements may be caused by complex interference corrections for these elements during SIMS analysis [see in "Secondary ion mass spectrometry (SIMS)" section]. Nevertheless, differences between V, Cr and Sc of Ti-poor and Ti-rich olivine are similar to that measured by SIMS. The contents of Co, Cu, Zn, As, Sb and Sn are similar in both olivine types.

Boron isotopes

Selected olivines (including the two porphyroclasts and one recrystallised olivine in Fig. 1f) were analysed in situ

Table 3 Trace element contents of olivine and serpentine by LA–ICP–MS

Section	Grain	Li	Al	Ca	Sc	Ti	V	Cr	Mn	Co	Cu	Zn	As	Sr	Y	Zr	Nb	Sn	Sb
VT8-3A	A-1	18	55	78	29	867	3.8	92	2,678	164	0.16	84	<0.05	2.0	0.51	1.12	0.049	0.52	0.004
VT8-3A	A-2	22	69	62	43	1,169	5.7	125	2,568	161	0.16	85	<0.05	1.6	0.42	1.23	0.052	0.54	0.004
VT8-3A	B-1	40	35	47	30	289	4.0	106	2,474	158	0.15	84	0.09	0.7	0.30	0.60	0.016	0.58	<0.003
VT8-3A	C-1	7	6	90	19	189	2.6	21	2,594	156	0.26	83	0.21	3.4	0.41	0.66	0.000	0.58	0.011
VT8-3A	E-1	9	<5	166	20	20	1.4	39	2,459	152	0.42	83	0.05	1.9	0.30	0.27	0.003	0.51	0.004
VT8-3A	G-1	6	<5	57	22	59	1.5	15	2,773	158	0.14	84	0.20	1.5	0.29	0.33	0.002	0.53	0.003
VT8-3A	G-2	3	<5	28	11	10	0.9	8	2,502	160	0.89	80	0.30	0.7	0.27	0.19	0.003	0.61	<0.003
VT8-3A	G-3	3	<5	21	14	30	1.1	9	2,378	157	0.11	78	0.21	0.3	0.15	0.10	0.000	0.60	<0.003
VT8-3A	G-4	12	<5	95	51	7	3.1	37	2,376	158	0.18	77	0.15	0.5	0.24	0.08	0.001	0.59	<0.003
VT8-3A	H-1	7	<5	118	21	80	0.9	14	2,613	164	0.22	79	0.14	3.6	0.65	0.81	0.012	0.45	0.004
VT8-3A	H-2	7	<5	46	20	62	0.8	28	2,736	158	0.14	83	0.10	1.1	0.43	0.71	0.005	0.56	0.013
VT8-3A	I-1	14	<5	70	22	108	2.7	65	2,442	153	0.14	82	<0.05	1.3	0.26	0.19	0.005	0.54	0.007
VT8-3A	I-2	21	<5	52	35	75	3.9	100	2,446	153	0.16	82	<0.05	1.0	0.26	0.17	0.001	0.58	0.004
VT8-3A	J-1	9	<5	74	17	44	2.1	38	2,540	158	0.24	85	0.09	2.3	0.30	0.35	0.001	0.50	<0.003
VT8-3A	J-2	6	<5	41	18	53	2.1	34	2,500	159	0.18	83	0.08	0.4	0.17	0.17	0.003	0.54	0.013

All concentrations in ppm

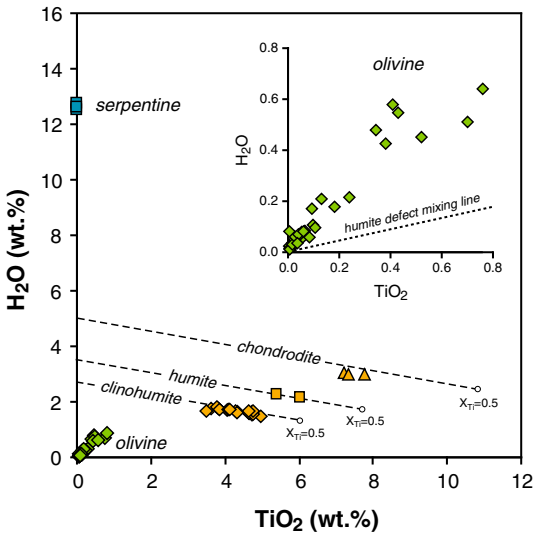

Fig. 2 TiO_2 versus H_2O for hydrous minerals from Voltri serpentinite. Olivine data measured by SIMS, serpentine and humite-group minerals by EPMA with water contents calculated from stoichiometry. Humite-group minerals (*orange symbols*) are subdivided into clinohumite, humite and chondrodite based on their chemistry. *Dashed lines* indicate predicted compositional variation in humite minerals following $TiO_2 = Mg(OH)_2$ exchange up to the maximum of $X_{Ti} = 0.5$. *Inset* shows detailed view of olivine compositions. Note the strong correlation between TiO_2 and H_2O for olivines, which follows a trend different than predicted for pure humite defects $MgTi[]O_2(OH)_2$

for boron isotopic composition by SIMS (Table 5). $\delta^{11}B$ values range from +17 to +23 ‰ and are on average the same for yellow Ti-rich olivine and colourless Ti-poor olivine. Variations up to 5 ‰ were observed within individual grains despite having constant major element compositions, which likely reflects variable fluid composition during the growth of secondary olivine.

Water content and structural position

Water contents of olivine measured with SIMS show a large variation from 100 ppm in Ti-poor olivine to 6,400 ppm in Ti-rich olivine. The values are high compared to typical mantle-derived olivine (<100 ppm; Peslier 2010). The high contents of water are not due to inclusions of hydrous minerals, such as serpentine and clinohumite, as these inclusions were avoided by using a small beam (<20 μm) and the shallow depth of penetration (<2 μm) during SIMS analysis. The H_2O contents show a strong positive correlation with TiO_2 contents (Fig. 2).

The structural position of OH was characterised using FTIR spectroscopy (Fig. 3). Five FTIR spectra obtained from optically clear areas of two grains (grains A and B) in a thick (150 μm) section show sharp absorption peaks at 3,687, 3,612, 3,564, 3,522 and 3,473 cm^{-1} and a broad peak around 3,400–3,415 cm^{-1} (Fig. 3). Although the beam was focused to 30 μm, the FTIR collects data through the entire thickness of sample; hence, it was unavoidable to measure minor inclusions. The peak at 3,687 cm^{-1} is related to serpentine inclusions (e.g., Kitamura et al. 1987; Matsyuk and Langer 2004; Khisina et al. 2008; Jung 2009), whereas the peak at 3,612 cm^{-1} is most likely related to OH incorporated as $Mg_2[]OH_4$, where [] represents an Si vacancy (Berry et al. 2005). The peaks at 3,564 and 3,522 cm^{-1} may be associated with Ti-clinohumite-type point defects composition of $MgTi[]O_2(OH)_2$ (Berry et al. 2005), although a peak position

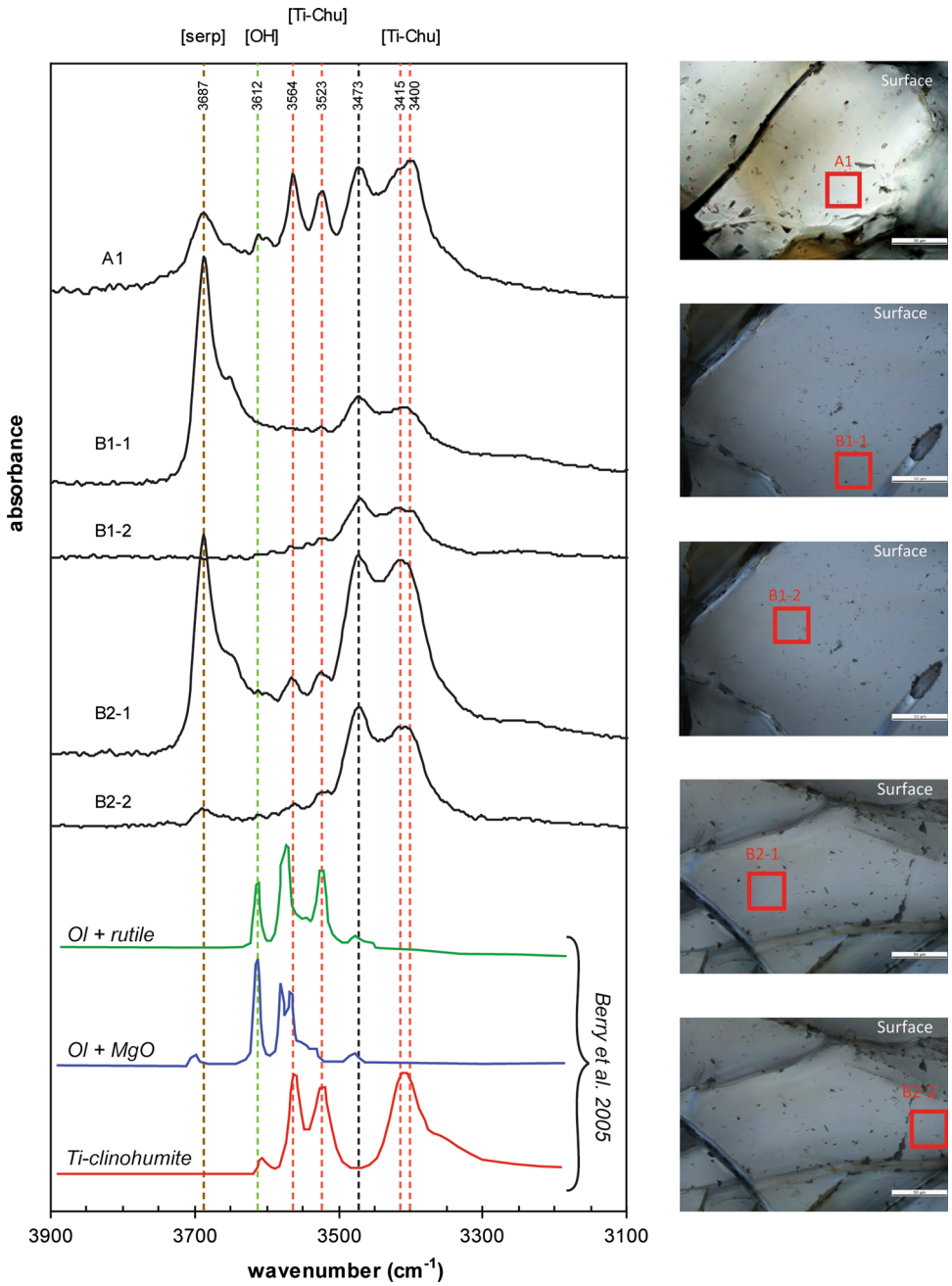

Fig. 3 FTIR spectra of two secondary olivine grains (**a**, **b**) from sample VT8-3. Drawn for comparison are spectra for Ti-clinohumite and olivine equilibrated with rutile (Ti–Chu vacancy) and periclase (Si vacancy) after Berry et al. (2005)

of at 3,572 cm^{-1} was reported by the authors. Alternatively, the FTIR spectra indicate the presence of Ti-clinohumite exsolutions or clustered planar defects (Matsyuk and Langer 2004), consistent with the broad peak around 3,400–3,415 cm^{-1} as well as the spectrum of pure Ti-clinohumite (Berry et al. 2005). However, Hermann et al. (2007) reported a peak at 3,564 cm^{-1} (not 3,572 cm^{-1}) for olivine that showed high densities of clustered planar Ti-clinohumite defects, which were imaged by TEM. It appears therefore difficult distinguish between defects and exsolutions based on FTIR data without additional TEM imaging. As Voltri olivines appeared homogeneous during EBSD and backscatter electron imaging at high magnifications, any exsolution of phases, if present, must be nanometre-scale.

The 3,473 cm^{-1} peak could not be related to any known OH-stretching modes in olivine or any known hydrous minerals or inclusions. A peak at 3,476–80 cm^{-1} has been attributed to Si vacancy substitution of hydrogen into olivine in previous studies (Lemaire et al. 2004; Bali et al. 2008; Kovacs et al. 2010). However, the peak reported by previous researchers is slightly offset from the one reported here and consistently very small relative to other peaks in contrast to the intense 3,473 cm^{-1} peak observed in our samples.

Ti-clinohumite and related minerals

The humite mineral group consists of four members with the general formula $n\mathrm{Mg_2SiO_4}\cdot\mathrm{Mg(F,OH)_2}$ where $n = 1$ for norbergite (Nrb), 2 for chondrodite (Chn), 3 for humite (Hu) and 4 for clinohumite (Chu) (Jones et al. 1969). Most natural humite-group minerals contain substantial amounts of TiO_2 (Evans and Trommsdorff 1983). Incorporation of TiO_2 up to $x = 0.5$ is accommodated by the exchange reaction $TiO_2 = Mg(OH)_2$, leading to the general formula $n\mathrm{Mg_2SiO_4}\cdot(1-x)\mathrm{Mg(OH,F)_2}\cdot x\mathrm{TiO_2}$. Note that the IMA reserves the names clinohumite for the F endmember and hydroxylclinohumite for the OH endmember (http://pubsites.uws.edu.au/ima-cnmnc/); for simplicity, the name clinohumite will be used throughout this article.

Humite-group minerals with their reddish brown colour were easily distinguishable under a microscope and were identified by their M/Si atomic ratio where M is the sum of all cations including Ti. The M/Si ratios are 2.25 for Chu, 2.33 for Hu and 2.5 for Chn. Ti-clinohumite is the most common humite-group mineral in sample VT8-3 (Fig. 1a, b, c, e). It occurs in contact with magnetite, antigorite and Ti-poor olivine. Small grains of chondrodite and humite were observed during the composition analysis with EPMA (Table 1; Fig. 2). They occur together with other humite-group minerals and serpentine; electron backscattered images suggest that most individual grains are homogeneous in compositions. Rare lamellar intergrowths of clinohumite and chondrodite are found in contact with Ti-poor olivine (Fig. 1e). There is no textural evidence suggesting the replacement of olivine by humite-group minerals and vice versa. None of humite-group minerals is in contact with Ti-rich olivine. The presence of humite together with other humite-group minerals is rarely reported. Apparent humite compositions can be obtained from fine-grained intergrowths of clinohumite and chondrodite (Wirth et al. 2001), but whereas lamellar intergrowths were occasionally observed in other grains (Fig. 1e), the humite grains were optically homogeneous.

All humite-group minerals in our sample have high TiO_2 contents (Chu: 3.6–4.9 wt%; Hu: 5.4–6.0 wt%; Chn: 7.2–7.8 wt%), which equals to a range of $x = 0.35$–0.46 in the general formula $n\mathrm{Mg_2SiO_4}\cdot(1-x)\mathrm{Mg(OH,F)_2}\cdot x\mathrm{TiO_2}$. They contain appreciable MnO (0.6–0.8 wt%), small amounts of Cr_2O_3 (0.01–0.18 wt%), and little Al_2O_3 (<0.07 wt%) and CaO (<0.01 wt%). Different humite-group minerals have similar major element compositions, including Mg# (85–87 for all). This is common for coexisting humite-group minerals, as shown in the Buell Park kimberlite, Arizona (Aoki et al. 1976), in serpentinised dunites from Isua, Greenland (Dymek et al. 1988) and ultra-high-pressure garnet pyroxenites from Dabie Shan, China (Hermann et al. 2007). The values of Mg# are similar to that of coexisting olivine. This is also observed in serpentinites elsewhere (Dymek et al. 1988, and references therein). Water contents based on stoichiometry (cf. Jones et al. 1969) are 1.5–1.8 wt% in clinohumite, 2.1–2.2 wt% in humite and 3.0 wt% in chondrodite. Water contents measured by SIMS give similar values (1.5–1.8, 2.0 and 2.6–3.0 wt%, respectively). Fluorine contents are low (0.03–0.11 wt%).

Trace element analysis revealed that humite-group minerals are enriched in volatiles and high-field strength elements (HFSE) (Table 4). Lithium contents (1–17 ppm) are lower, whereas B contents (21–43 ppm) are higher than coexisting olivine (4–48 and 9–22 ppm, respectively). Zirconium contents are rather high (12–126 ppm), whereas V (2–24 ppm), Sr (1–4 ppm) and Y (0.3–2 ppm) contents are similar to those observed in olivine. Apart from slightly higher F contents of chondrodite, trace elements show little difference between various humite minerals.

Serpentine

Serpentine (antigorite) has a narrow range of Mg# (94.5–94.8) and contains 1.3–2.6 wt% Al_2O_3 and 0.1–0.2 wt% Cr_2O_3. Some MnO (0.01–0.05 wt%) and NiO (0.07–0.17) were also detected. Compared to coexisting olivine, it has low contents of Ti (8–13 ppm), Li (<0.15 ppm) and B (6–9 ppm), whereas F contents (15–47 ppm) fall within the same range.

Clinopyroxene

Two types of clinopyroxene are present. The first type is coarse-grained deformed augite, which exhibits well-developed cleavages. Its Mg# falls between 90.6 and 91.8, and it contains 4.9–7.2 wt% Al_2O_3, 1.0–1.2 wt% Cr_2O_3, 0.3–0.5 wt% TiO_2 and 0.3–0.4 wt% Na_2O. The high concentrations of Ti, Al and Cr suggest this type of clinopyroxene to be of relic mantle origin and survived serpentinisation.

In contrast, the second type has an acicular habit and is often associated with clinohumite-rich domains. It is nearly pure diopside, with high Mg # (94.3–96.4) and low TiO_2 (<0.01–0.4 wt%), Al_2O_3 (0.03–0.66 wt%), Cr_2O_3 (0.02–0.3 wt%) and Na_2O (0.1–0.3 wt%) and is therefore considered to be of metamorphic origin.

Oxides

Oxides (var. magnetite) are closely associated with clinohumite-rich veins, but also occur within large patches of secondary olivine. They contain significant Cr_2O_3 (3.5–6.1 wt%) but low TiO_2 (<0.5 wt%) and MnO (<0.1 wt%). In addition, they contain ca. 0.07 wt% V_2O_3,

Table 4 Trace element and H_2O contents of humite-group minerals and serpentine by SIMS

Section	Grain	H_2O wt%	TiO_2 wt%	Li ppm	B ppm	F ppm	V ppm	Cr ppm	Mn ppm	Sr ppm	Y ppm	Zr ppm
Clinohumite												
VT8-3B	C-1	1.7	4.2	9	29	472	9	581	5,364	1.3	0.4	16
VT8-3B	C-2	1.8	3.9	6	40	335	16	759	6,020	1.3	0.6	25
VT8-3B	C-3	2.1	3.6	1	32	416	2	56	5,690	0.9	0.5	26
VT8-3B	A-1	1.8	3.6	2	43	751	11	387	3,366	1.2	1.2	51
VT8-3B	H-1	1.8	4.2	17	32	725	21	599	4,412	0.9	0.5	12
VT8-3C	J-1	1.5	3.8	1	36	675	6	59	4,323	0.7	0.3	12
Humite												
VT8-3B	A-2	2.0	5.5	5	22	616	19	391	3,729	1.5	1.8	13
VT8-3C	I-1	2.0	5.9	14	33	805	12	811	3,658	1.4	1.0	25
Chondrodite												
VT8-3B	C-4	2.9	7.0	7	21	596	7	851	6,088	1.3	0.5	20
VT8-3B	C-5	3.0	6.3	12	28	669	5	1,237	4,751	4.4	0.7	39
VT8-3B	H-2	2.6	7.4	6	29	1,129	24	536	4,653	0.9	1.0	126
VT8-3C	K-1	3.0	7.0	6	36	1,116	12	527	4,375	2.2	0.5	30
Antigorite												
VT8-3A	E-1	11.7	0.002	0.1	6	17			305	0.3	0.6	0.8
VT8-3B	D-1	18.5	0.001	0.1	10	85	103	2,298	301	0.6	0.5	0.7
VT8-3B	A-1	13.3	0.002	0.1	10	335	73	2,103	257	0.4	0.5	0.5

0.10 wt% NiO and <0.01 wt% ZnO. No chromite was observed in the sample.

Interpretation and discussion

Origin of high Ti and H_2O in olivine

The good positive correlation between H_2O and TiO_2 contents of secondary metamorphic olivine from Voltri (Fig. 2) suggests that these elements are incorporated by a common mechanism. FTIR spectra of olivine indeed indicated the presence of Ti-clinohumite planar defects or exsolutions (in "Water content and structural position" section). However, Voltri olivines have excess water compared to pure Ti-humite defects as well as Ti-clinohumite grains in the sample matrix (Fig. 2), which suggests that the planar defects or exsolutions must have a composition that differs from the ideal formula of $MgTi[]O_2(OH)_2$. FTIR spectra do show an abundance of serpentine microinclusions in addition to clinohumite defects or exsolutions, which could explain the increased H_2O signal, but such inclusions were effectively avoided during SIMS analyses. We therefore infer that olivine contains clinohumite defects or exsolutions with considerably less Ti than the ideal formula $MgTi[]O_2(OH)_2$. Based on the relative amounts of TiO_2 and H_2O in olivine, we derive a value of ca. 0.1 for x in the formula $(1-x)Mg(OH)_2{\cdot}xTiO_2$. This value is significantly less than that of humite-group minerals in the sample matrix, which have a value of x ranging from 0.34 to 0.46.

Very high solubility of H_2O in olivine under water-saturated conditions was indicated by experimental data at high pressures (e.g., Kohlstedt et al. 1996 report up to 0.5 wt% H_2O at 13 GPa). On the other hand, water contents of mantle olivines are typically <100 ppm, with an average of 43 ppm calculated based on water contents of mantle-derived melts (Peslier 2010). The maximum solubility of TiO_2 in olivine is ca. 1.3 wt% in anhydrous systems at temperatures in excess of 1,200 °C (Hermann et al. 2005) but are strongly controlled by coexisting Ti-bearing phases. Solubility is ca. 0.2 wt% in natural water-bearing systems containing ilmenite at 1,200 °C (Ulmer et al. 1998). Olivines from mantle xenoliths have maximum TiO_2 contents of ca. 0.06 wt% (De Hoog et al. 2010). Our results indicate that the presence of clinohumite defects or nano-exsolutions can accommodate H_2O and TiO_2 in olivine well above those of typical mantle values. Hermann et al. (2007) pointed out that the humite-group minerals and olivine form a polysomatic series with decreasing hydrous interlayers relative to olivine layers going from norbergite ($n = 1$) to clinohumite ($n = 4$) to olivine ($n = \infty$). If TiO_2-rich olivines from Voltri are expressed using the general formula for humite-group minerals, $nMg_2SiO_4{\cdot}(1-x)Mg(OH)_2{\cdot}xTiO_2$, where $n = 4$ for

clinohumite and ∞ for pure olivine, the value for *n* reaches a minimum value of 16 for Voltri olivine.

High TiO_2 contents of olivine have been used to infer an ultradeep origin of rocks, as typical mantle olivine has Ti concentrations less than 350 ppm or ca. 0.06 wt% (Hermann et al. 2005; De Hoog et al. 2010). For example, Ti contents of over 0.6 wt% and rutile/ilmenite exsolutions in olivines from garnet peridotites from Alpe Arami were used to infer an origin in excess of 300 km (Dobrzhinetskaya et al. 1996), although the pressure dependence of Ti solubility was later questioned by experiments by Hermann et al. (2005). In addition, olivine with 0.19 wt% TiO_2 was reported by Hermann et al. (2007) as a breakdown product of Ti-chondrodite under high pressure in garnet pyroxenites from Dabie Shan UHP belt. The Ti contents of olivine in our sample (up to 0.9 wt%) indicate that olivine containing even higher TiO_2 contents can be formed at relatively moderate pressures and temperatures (600 °C and 25 kbar; Scambelluri et al. 1995). Thus, even such high TiO_2 contents of olivine cannot be used to demonstrate deep mantle conditions.

Formation conditions of Ti-rich hydrous olivine and humite-group minerals

The peak P–T conditions, 600 °C and 25 kbar, of the metaperidotite were estimated from boudins of metagabbros (Scambelluri et al. 1995). This agrees with the assemblage Atg + Fo + Ti–Chu + Di of the metaperidotite. The stability field is bracketed by the antigorite-out reaction (Atg + Di = Fo + Tr + H_2O) and the brucite-out reaction (Atg + Brc = Fo + H_2O). Since antigorite breaks down to olivine and orthopyroxene at high pressures, the upper stability limit is defined by Atg = Fo + En + H_2O. Some minor secondary Opx was reported in these rocks by Scambelluri et al. (1995).

The upper stability limit of Ti-clinohumite is provided by the breakdown reaction Ti–Chu = Fo + Gk ($MgTiO_3$) + H_2O, which is close to the antigorite stability limit in F-free assemblages (Engi and Lindsley 1980; Trommsdorff and Evans 1980; Weiss 1997). The absence in our samples of geikielite ($MgTiO_3$), a breakdown product of clinohumite commonly reported from other ultramafic localities (Trommsdorff and Evans 1980; Okay 1994; Sanchez-Vizcaino et al. 2005; e.g., Hermann et al. 2007) limits the temperature of the formation to below ca. 675 °C (Engi and Lindsley 1980).

A distinctive feature of our sample is the occurrence of abundant Ti-chondrodite (ca. 25 % of all humite-group minerals). Unfortunately, the relative stability of different humite-group minerals is not well constrained. Chondrodite may form preferentially in Mg-rich rocks (Mg# > 95; Engi and Lindsley 1980; Dymek et al. 1988), but our sample has relatively low Mg# of 86–87. Engi and Lindsley (1980) suggested that chondrodite is stable at higher pressures than clinohumite. Thus, re-equilibration during exhumation would form clinohumite at the expense of chondrodite, but microtextures in our sample show no clear evidence of humite-group minerals replacing each other. Weiss (1977) showed that temperature may play an important role, as clinohumite breaks down to more Ti-rich norbergite and olivine (+fluid) with increasing temperature over a narrow 20 °C interval. Taking into account the proximity of Voltri P–T conditions to the start of the F-free clinohumite breakdown reaction, we infer that clinohumite started to break down to chondrodite and olivine according the reaction Ti–OH–Chu = Ti–OH–Chn + 2 Ol, but that the temperature (ca. 600 °C; Scambelluri et al. 1995) was not high enough for further breakdown to ilmenite and fluid.

The conditions and timing of the formation of Ti-rich olivine relative to formation of Ti-clinohumite are not clear. Previously reported occurrences of high-TiO_2 olivine are in chlorite harzburgites from the Almirez Massif in Spain (Trommsdorff et al. 1998; Ruiz Cruz et al. 1999; Puga et al. 1999; Garrido et al. 2005; Sanchez-Vizcaino et al. 2005) and in garnet pyroxenites from Dabie Shan UHP belt, China (Hermann et al. 2007). In the Almirez Massif, brown olivine is intergrown with Ti-clinohumite and contains numerous Ti-rich solid inclusions. It is interpreted to be the breakdown product of clinohumite, which still partially survived as lamellae and patchy inclusions in olivine. An origin of Ti-rich olivine as a breakdown product of Ti-clinohumite and Ti-chondrodite was also proposed for garnet pyroxenites from Dabie Shan (Hermann et al. 2007). In contrast, Ti-rich yellow olivine documented here from Voltri appears to have a different origin, as it occurs away from Ti-clinohumite-rich domains, contains no lamellae or patchy inclusions of clinohumite and lacks inclusions of Mg-rich ilmenite (a breakdown product of Ti-clinohumite). In addition, olivine closely associated with humite-group minerals is Ti-poor. Ti-rich olivine forms overgrowths on Ti-poor olivine, but humite-group minerals do not occur in contact with Ti-rich olivine. In Voltri, clinohumite typically occurs in veins hosted by massive antigorite, which formed during prograde Alpine subduction and deformation (Scambelluri et al. 1995; Scambelluri and Rampone 1999). Hence, clinohumite formed together with metamorphic olivine during dehydration near peak pressures of 18–25 kbar. Since peridotites originally contain low TiO_2, variable influx of fluids from external rocks during prograde metamorphism may have resulted in formation of Ti-poor olivine, Ti-rich olivine and Ti-clinohumite in the same sample.

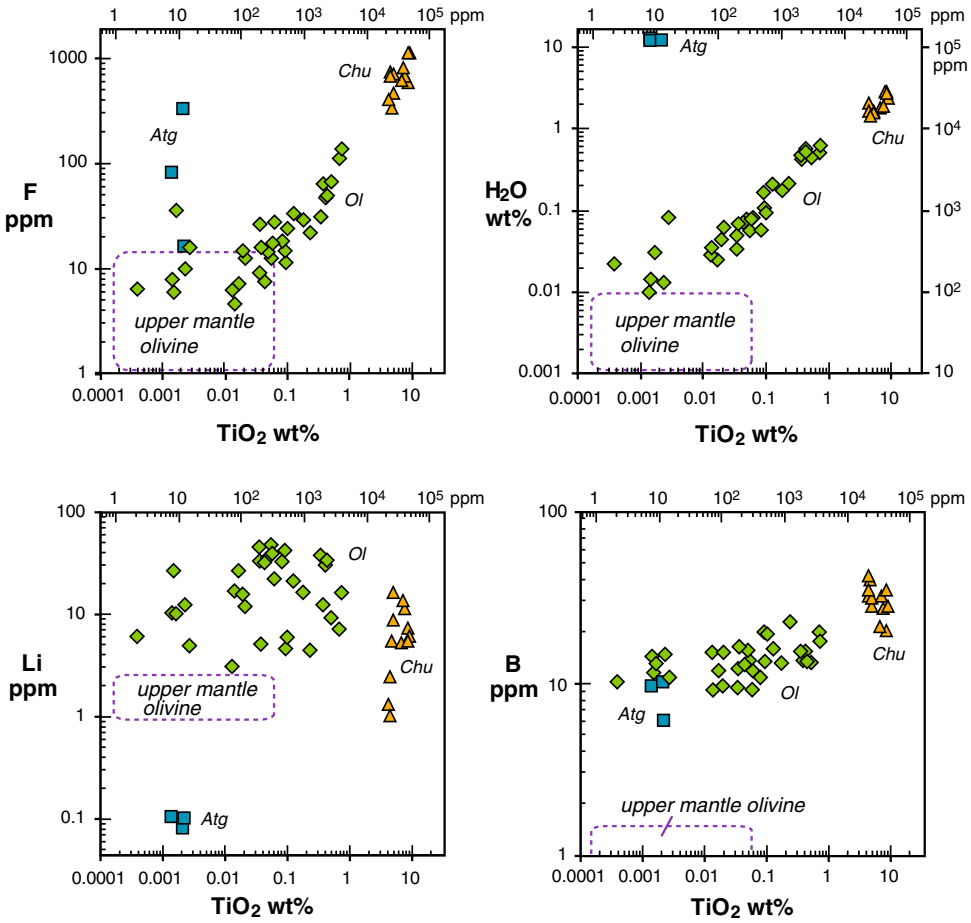

Fig. 4 TiO_2 versus fluid-mobile elements F, H_2O, Li and B for olivine (Ol), antigorite (Atg) and humite-group minerals (Chu). Fields for mantle olivine values compiled from Kent and Rossman (2002), Guggino et al. (2007), De Hoog et al. (2010) and Peslier (2010)

Implications for transfer of water, HFSE and fluid-mobile elements beyond arc depths

Our results indicate that secondary olivine which formed during subduction dehydration of serpentinite may contain considerable amounts of H_2O and TiO_2 and may therefore play an important role in the redistribution of these elements in subduction zones. Fluorine in olivine behaves similar to H_2O as it shows a similar positive correlation with TiO_2 (Fig. 4). As F contents fall in-between typical mantle olivine values (0.5–14 ppm; Guggino et al. 2007) and humite-group minerals, we suspect that F enters humite defects in olivine. Similarly, the contents of Zr and Nb positively correlate with TiO_2 contents, which probably reflect HFSE partitioning into Ti-clinohumite defects in olivine. As both F and HFSE are considerably enriched in secondary olivine, anomalously high contents of these elements can be introduced into the mantle. Likewise, Garrido et al. (2005) reported chloritised harzburgite from the Almirez Massif acting as a sink for HFSE during dehydration of serpentinite. The main carriers of HSFE in their study were Cr-magnetite and ilmenite exsolutions in brown olivine containing Ti-clinohumite intergrowths (Ruiz Cruz et al. 1999; Garrido et al. 2005). Although metamorphic conditions in Voltri were not high enough to reach Ti-clinohumite breakdown (Scambelluri et al. 1995), our observations are similar to those of Garrido et al. (2005); hence, HFSE enrichment in the secondary olivine may be important in understanding the distribution of these elements, as they have been shown to be mobile in subducting slabs at depths below volcanic arcs (Gao et al. 2007). Upon deeper subduction, increasing temperatures lead to breakdown of Ti-clinohumite defects and formation of Mg-rich ilmenite (Puga et al. 1999; Risold et al. 2001; Hermann et al. 2007), which will retain HFSE in the rock. Also, inclusions and humite-type defects likely remain stable in olivine under high pressures (Kitamura et al. 1987; Wirth et al. 2001; Matsyuk and Langer 2004).

In contrast to HFSE and F, Li shows no correlation with TiO_2 content in olivine. It is enriched in both Ti-poor and Ti-rich olivine compared with antigorite and clinohumite, as well as typical upper mantle olivine (Fig. 4). As antigorite has low Li contents and its breakdown can liberate only little Li, this requires an alternative source of Li in olivine during serpentinite dehydration. Possible sources are the breakdown of relic mantle Cpx and external fluids.

Table 5 Boron isotope compositions of olivine by SIMS

Section	Grain	B (ppm)	δ^{11}B ‰ SRM951	δ^{11}B 1 s ‰
VT8-3B	F-1-1 (Ti-rich porphyroclast)	10.1	+18.7	±1.3
VT8-3B	F-1-2	12.0	+18.9	±1.1
VT8-3B	F-1-3	14.0	+17.4	±1.0
VT8-3B	F-2-1 (Ti-poor recrystallised)	17.3	+22.7	±0.8
VT8-3B	F-3-1 (Ti-poor porphyroclast)	13.6	+22.0	±1.1
VT8-3B	F-3-2	15.2	+17.3	±1.1
VT8-3B	I-1 (Ti-poor matrix)	10.5	+16.7	±1.3
Average		13.3	+19.1	±2.4

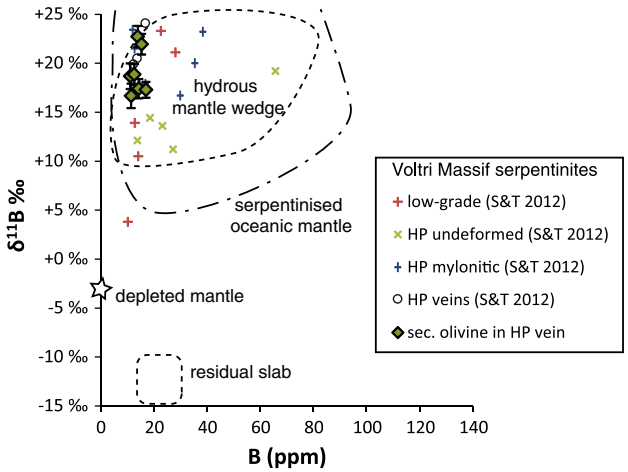

Fig. 5 Boron isotopes versus B concentrations for Voltri secondary olivine (this study) and Voltri HP serpentinites (Scambelluri and Tonarini 2012). Fields for subducted oceanic crust and hydrated mantle wedge after Scambelluri and Tonarini (2012), serpentinised oceanic mantle (which extend up to +40 ‰) and depleted mantle after Vils et al. (2009) and references therein

Relic clinopyroxene in VT8-3 contains only 5–9 ppm Li, considerable lower than Ti-rich olivine, and therefore, an unlikely source of Li found in olivine. External fluids may be derived from gabbros and mafic volcanic rocks during eclogitisation (Scambelluri and Rampone 1999; Scambelluri et al. 2004a).

The behaviour of B during serpentine dehydration is of particular interest as its behaviour in arc settings is thought to be dominated by serpentinite (Scambelluri and Tonarini 2012). Similar to Li, B is enriched in Ti-poor as well as Ti-rich olivine compared with antigorite. Its abundance in olivine is therefore related not only to the presence of Ti-clinohumite exsolutions but also to a distinct solution mechanism such as B(OH) = SiO (Sykes et al. 1994). The B contents are considerably higher than typical mantle values (Fig. 4), in agreement with Scambelluri et al. (2004b) who observed high residual B contents in dehydrated serpentinites of ca. 10 ppm. Boron isotope compositions show high δ^{11}B (+17 to +23 ‰, Table 5) compared with typical mantle values of ca. −3 ‰ (Hart et al. 1999). The observed values for the metamorphic olivine are virtually identical to the bulk-rock data for the high-pressure veins from which our sample is derived (Fig. 5; +20 to +24 ‰, Scambelluri and Tonarini, 2012). Scambelluri and Tonarini (2012) consider the high δ^{11}B values due to a supra-subduction zone setting of the serpentinites, although similar values (+5 to +40 ‰) have been reported for sea-floor altered serpentinites (Vils et al. 2009). Scambelluri and Tonarini (2012) reported little fractionation of B isotopes with increasing metamorphic grade of serpentinites and little B loss during transition from lizardite to antigorite. Our olivine data confirm retention of B and limited B isotopic fractionation during the metamorphic transformation of serpentine to olivine, so that even after complete dehydration the residue will retain its B isotope signature. Therefore, subduction of secondary olivine may introduce significant B isotope anomalies into the deep mantle.

Finally, the deep subduction of serpentinites and their dehydration may contribute to redox changes in the Earth's mantle. Serpentinisation, the hydration of peridotites, is accompanied by the oxidation of Fe to form magnetite and the release of reduced gases, such as H_2 and CH_4 (Evans 2008). In reverse dehydration reaction, H_2O-rich olivine is formed and may be subducted to even deeper mantle. When such olivine comes in contact with hot dry peridotites, it may readily release H_2, as diffusion rate for hydrogen is much higher than those of metals in olivine (Ingrin and Skogby 2000; Hwang et al. 2008). In addition, at the reducing lower mantle conditions, H_2 is immiscible with hydrous fluids (Bali et al. 2013). Thus, fluid released from subducted hydrous olivine may lead to reduced mantle domains, and, together with carbon brought down by sinking slabs, it may induce favourable conditions for the formation of diamond.

Summary

Secondary (metamorphic) olivine in dehydrating serpentinite from the high-pressure Voltri complex is enriched in H_2O (up to 0.7 wt%) and TiO_2 (up to 0.86 wt%); the two show a positive correlation in their concentrations. Based on FTIR data, we suggest that these elements are hosted by clustered planar Ti-clinohumite defects or nanoscale exsolutions in olivine.

Secondary metamorphic olivine is significantly enriched in Li (2–60 ppm), B (10–20 ppm), F (10–130 ppm) and Zr (0.9–2.1 ppm) compared with mantle olivine. It shows high

$\delta^{11}B$ values ranging from +17 to +23 ‰, which are similar to those of bulk serpentinites. The dehydration of serpentine to form olivine did not release much of B and F. Our data indicate that secondary olivine may play a significant role in transporting HFSE, water, fluid-mobile elements and ^{11}B to the deep mantle. Release of hydrogen from subducted hydrous olivine in the deep mantle may result in strongly reducing mantle domains.

Acknowledgments We thank Byeongkwan Ko at Seoul National University for assistance with FTIR analysis, Nicola Kayzer at University of Edinburgh for assistance with EBSD analysis, Richard Hinton and John Craven at the Edinburgh Ion Microprobe Facility for technical support and Richard Brooker at University of Bristol for discussions about olivine FTIR spectra. Constructive reviews by István Kovács and Marco Scambelluri are gratefully acknowledged. Jacques Touret is thanked for editorial handling and helpful suggestions. H.J. was supported by the Mid-career Research Program through an NRF grant funded by the MEST (3345-20130011) in Korea.

References

Aoki K, Fujino K, Akaogi M (1976) Titanochondrodite and titanoclinohumite derived from upper mantle in Buell Park kimberlite, Arizona, USA. Contrib Mineral Petrol 56:243–253

Bali E, Bolfan-Casanova N, Koga KT (2008) Pressure and temperature dependence of H solubility in forsterite: an implication to water activity in the Earth interior. Earth Planet Sci Lett 268:354–363

Bali E, Audétat A, Keppler H (2013) Water and hydrogen are immiscible in Earth's mantle. Nature 495:220–222

Berry AJ, Hermann J, O'Neill HSC, Foran GJ (2005) Fingerprinting the water site in mantle olivine. Geology 33:869–872

Catanzaro EJ, Champion CE, Garner EL, Marinenko G, Sappenfield KM, Shields WR (1970) Standard reference materials: boric acid; isotopic and assay standard reference materials. NBS Special Publication 260-17, 70 p. http://www.nist.gov/srm/upload/SP260-17.PDF

Cimmino F, Messiga B, Piccardo GB, Zeda O (1979) Titanian clinohumite-bearing assemblages within antigorite serpentinites of the Voltri Massif (Western Liguria): influence on the geodynamic evolution of Piemontese ultramafic sections. Ofioliti 4:97–120

De Hoog JCM, Gall L, Cornell DH (2010) Trace-element geochemistry of mantle olivine and application to mantle petrogenesis and geothermobarometry. Chem Geol 270:196–215

Dobrzhinetskaya L, Green HW, Wang S (1996) Alpe Arami: a peridotite massif from depths of more than 300 kilometers. Science 271:1841–1845

Dymek RF, Boak JL, Brothers SC (1988) Titanian chondrodite-bearing and titanian clinohumite-bearing metadunite from the 3800 Ma Isua supracrustal belt, West Greenland—chemistry, petrology, and origin. Am Mineral 73:547–558

Engi M, Lindsley DH (1980) Stability of titanian clinohumite—experiments and thermodynamic analysis. Contrib Mineral Petrol 72:415–424

Evans BW (2008) Control of the products of serpentinization by the $Fe^{2+}Mg_{-1}$ exchange potential of olivine and orthopyroxene. J Petrol 49:1873–1887

Evans BW, Trommsdorff V (1983) Fluorine hydroxyl titanian clinohumite in Alpine recrystallized garnet peridotite: compositional controls and petrologic significance. Am J Sci 283-A:355–369

Gao J, John T, Klemd R, Xiong XM (2007) Mobilization of Ti-Nb-Ta during subduction: evidence from rutile-bearing dehydration segregations and veins hosted in eclogite, Tianshan, NW China. Geochim Cosmochim Acta 71:4974–4996

Garrido CJ, Sanchez-Vizcaino VL, Gomez-Pugnaire MT, Trommsdorff V, Alard O, Bodinier JL, Godard M (2005) Enrichment of HFSE in chlorite-harzburgite produced by high-pressure dehydration of antigorite-serpentinite: implications for subduction magmatism. Geochem Geophys Geosyst 6:Q01J15. doi:10.1029/2004GC000791

Guggino SN, Hervig RL, Bell DR (2007) Fluorine in olivines from plutonic, extrusive, and hypabyssal suites (abstract). Eos Trans Am Geophys Union 88, Fall Meet Suppl, V41B-0609

Hall L (1998) The effect of water on mantle melting. Unpublished PhD thesis, Bristol University

Hart SR, Blusztajn J, Dick HJB, Meyer PS, Muehlenbachs K (1999) The fingerprint of seawater circulation in a 500-meter section of ocean crust gabbros. Geochim Cosmochim Acta 63:4059–4080

Hattori KH, Guillot S (2003) Volcanic fronts form as a consequence of serpentinite dehydration in the forearc mantle wedge. Geology 31:525–528

Hattori KH, Guillot S (2007) Geochemical character of serpentinites associated with high-to ultrahigh-pressure metamorphic rocks in the Alps, Cuba, and the Himalayas: recycling of elements in subduction zones. Geochem Geophys Geosyst 8:Q09010. doi:10.1029/2007gc001594

Hermann J, O'Neill HSC, Berry AJ (2005) Titanium solubility in olivine in the system TiO_2–MgO–SiO_2: no evidence for an ultra-deep origin of Ti-bearing olivine. Contrib Mineral Petrol 148:746–760

Hermann J, Gerald JDF, Malaspina N, Berry AJ, Scambelluri M (2007) OH-bearing planar defects in olivine produced by the breakdown of Ti-rich humite minerals from Dabie Shan (China). Contrib Mineral Petrol 153:417–428

Hwang SL, Yui TF, Chu HT, Shen PY, Iizuka Y, Yang HY, Yang JS, Xu ZQ (2008) Hematite and magnetite precipitates in olivine from the Sulu peridotite: a result of dehydrogenation-oxidation reaction of mantle olivine? Am Mineral 93:1051–1060

Ingrin J, Skogby H (2000) Hydrogen in nominally anhydrous upper-mantle minerals: concentration levels and implications. Eur J Mineral 12:543–570

Jarosewich E, Nelen J, Norber J (1980) Reference samples for electron probe analysis. Geostandards Newsl 4:43–47

Jochum KP, Nohl U (2008) Reference materials in geochemistry and environmental research and the GeoReM database. Chem Geol 253:50–53

John T, Scambelluri M, Frische M, Barnes JD, Bach W (2011) Dehydration of subducting serpentinite: implications for halogen mobility in subduction zones and the deep halogen cycle. Earth Planet Sci Lett 308:65–76

Jones NW, Ribbe PH, Gibbs GV (1969) Crystal chemistry of humite minerals. Am Mineral 54:391–411

Jung H (2009) Deformation fabrics of olivine in Val Malenco peridotite found in Italy and implications for the seismic anisotropy in the upper mantle. Lithos 109:341–349

Kent AJR, Rossman GR (2002) Hydrogen, lithium, and boron in mantle-derived olivine: the role of coupled substitutions. Am Mineral 87:1432–1436

Khisina NR, Wirth R (2002) Hydrous olivine $(Mg_{1-y}Fe^{2+}_y)_{2-x}V_xSiO_{4-}H_{2x}$—a new DHMS phase of variable composition observed as nanometer-sized precipitations in mantle olivine. Phys Chem Minerals 29:98–111

Khisina N, Wirth R, Matsyuk S, Koch-Muller M (2008) Microstructures and OH-bearing nano-inclusions in "wet" olivine xenocrysts from the Udachnaya kimberlite. Eur J Mineral 20:1067–1078

Kitamura M, Kondoh S, Morimoto N, Miller GH, Rossman GR, Putnis A (1987) Planar OH-bearing defects in mantle olivine. Nature 328:143–145

Kodolanyi J, Pettke T, Spandler C, Kamber BS, Gmeling K (2012) Geochemistry of ocean floor and fore-arc serpentinites: constraints on the ultramafic input to subduction zones. J Petrol 53(2):235–270

Kohlstedt DL, Keppler H, Rubie DC (1996) Solubility of water in the alpha, beta and gamma phases of $(Mg, Fe)_2SiO_4$. Contrib Mineral Petrol 123:345–357

Kovacs I, O'Neill HSC, Hermann J, Hauri EH (2010) Site-specific infrared O–H absorption coefficients for water substitution into olivine. Am Mineral 95:292–299

Lemaire C, Kohn SC, Brooker RA (2004) The effect of silica activity on the incorporation mechanisms of water in synthetic forsterite: a polarised infrared spectroscopic study. Contrib Mineral Petrol 147:48–57

Matsyuk SS, Langer K (2004) Hydroxyl in olivines from mantle xenoliths in kimberlites of the Siberian platform. Contrib Mineral Petrol 147:413–437

Okay AI (1994) Sapphirine and Ti-clinohumite in ultra-high-pressure garnet-pyroxenite and eclogite from Dabie-Shan, China. Contrib Mineral Petrol 116:145–155

Pearce NJG, Perkins WT, Westgate JA, Gorton MP, Jackson SE, Neal CR, Chenery SP (1997) A compilation of new and published major and trace element data for NIST SRM 610 and NIST SRM 612 glass reference materials. Geostandards Newsl 21:115–144

Peslier AH (2010) A review of water contents of nominally anhydrous natural minerals in the mantles of Earth, Mars and the Moon. J Volcanol Geotherm Res 197:239–258

Piccardo GB, Rampone E, Scambelluri M (1988) The Alpine evolution of the Erro-Tobio peridotites (Voltri Massif-Ligurian Alps): some field and petrographic constraints. Ofioliti 13:169–174

Puga E, Cruz MDR, De Federico AD (1999) Magnetite-silicate inclusions in olivine of ophiolitic metagabbros from the Mulhacen Complex, Betic Cordillera, southeastern Spain. Can Mineral 37:1191–1209

Risold AC, Trommsdorff V, Grobety B (2001) Genesis of ilmenite rods and palisades along humite-type defects in olivine from Alpe Arami. Contrib Mineral Petrol 140:619–628

Rosner M, Meixner A (2004) Boron isotopic composition and concentration of ten geological reference materials. Geostand Geoanal Res 28:431–441

Rosner M, Wiedenbeck M, Ludwig T (2008) Composition-induced variations in SIMS instrumental mass fractionation during boron isotope ratio measurements of silicate glasses. Geostand Geoanal Res 32:27–38

Ruiz Cruz MD, Puga E, Nieto JM (1999) Silicate and oxide exsolution in pseudo-spinifex olivine from metaultramafic rocks of the Betic Ophiolitic Association: a TEM study. Am Mineral 84:1915–1924

Sanchez-Vizcaino VL, Trommsdorff V, Gomez-Pugnaire MT, Garrido CJ, Muntener O, Connolly JAD (2005) Petrology of titanian clinohumite and olivine at the high-pressure breakdown of antigorite serpentinite to chlorite harzburgite (Almirez Massif, S. Spain). Contrib Mineral Petrol 149:627–646

Savov IP, Ryan JG, D'Antonio M, Fryer P (2007) Shallow slab fluid release across and along the Mariana arc-basin system: insights from geochemistry of serpentinized peridotites from the Mariana fore arc. J Geophys Res Solid Earth 112:B09205. doi:10.1029/2006jb004749

Scambelluri M, Rampone E (1999) Mg-metasomatism of oceanic gabbros and its control on Ti-clinohumite formation during eclogitization. Contrib Mineral Petrol 135:1–17

Scambelluri M, Tonarini S (2012) Boron isotope evidence for shallow fluid transfer across subduction zones by serpentinized mantle. Geology 40:907–910

Scambelluri M, Strating EHH, Piccardo GB, Vissers RLM, Rampone E (1991) Alpine olivine-bearing and titanian clinohumite-bearing assemblages in the Erro-Tobbio peridotite (Voltri-Massif, NW Italy). J Metamorph Geol 9:79–91

Scambelluri M, Muntener O, Hermann J, Piccardo GB, Trommsdorff V (1995) Subduction of water into the mantle—history of an Alpine peridotite. Geology 23:459–462

Scambelluri M, Fiebig J, Malaspina N, Muntener O, Pettke T (2004a) Serpentinite subduction: implications for fluid processes and trace-element recycling. Int Geol Rev 46:595–613

Scambelluri M, Muntener O, Ottolini L, Pettke TT, Vannucci R (2004b) The fate of B, Cl and Li in the subducted oceanic mantle and in the antigorite breakdown fluids. Earth Planet Sci Lett 222:217–234

Shishkina TA, Botcharnikov RE, Holtz F, Almeev RR, Portnyagin MV (2010) Solubility of H_2O- and CO_2-bearing fluids in tholeiitic basalts at pressures up to 500 MPa. Chem Geol 277:115–125

Sykes D, Rossman GR, Veblen DR, Grew ES (1994) Enhanced H and F incorporation in borian olivine. Am Mineral 79:904–908

Trommsdorff V, Evans BW (1980) Titanian hydroxyl-clinohumite—formation and breakdown in antigorite rocks (Malenco, Italy). Contrib Mineral Petrol 72:229–242

Trommsdorff V, Sanchez-Vizcaino VL, Gomez-Pugnaire MT, Muntener O (1998) High pressure breakdown of antigorite to spinifex-textured olivine and orthopyroxene, SE Spain. Contrib Mineral Petrol 132:139–148

Ulmer P, Trommsdorff V (1995) Serpentine stability to mantle depths and subduction-related magmatism. Science 268:858–861

Ulmer P, Risold AC, Trommsdorff V (1998) TiO_2 solubility in mantle olivine as a function of pressure, temperature, a_{SiO2}, and f_{H2} (abstract). EOS Trans Am Geophys Union 79, Spring Meet Suppl, M31A-07

Vils F, Tonarini S, Kalt A, Seitz HM (2009) Boron, lithium and strontium isotopes as tracers of seawater-serpentinite interaction at Mid-Atlantic ridge, ODP Leg 209. Earth Planet Sci Lett 286:414–425

Weiss M (1997) Clinohumites: a field and experimental study. Ph.D. Thesis, ETH Zurich

Whitney DL, Evans BW (2010) Abbreviations for names of rock-forming minerals. Am Mineral 95:185–187

Wirth R, Dobrzhinetskaya LF, Green HW (2001) Electron microscope study of the reaction olivine plus $H_2O + TiO_2 \rightarrow$ titanian clinohumite plus titanian chondrodite synthesized at 8 GPa, 1300 K. Am Mineral 86:601–610